Heat and Mass Transfer (2026) 62:71
https://doi.org/10.1007/s00231-026-03702-8

RESEARCH

Experimental investigation on critical heat flux and upstream-CHF with R-134a at high pressures

Nikolai Rensch[1] · Aurelian Florin Badea[1] · Xu Cheng[1]

Received: 3 February 2026 / Accepted: 8 May 2026

Abstract

An experimental study of the critical heat flux (CHF) in R-134a was performed in a vertical round tube with upward flow. The experiments were conducted over a wide pressure range from 1.10 MPa to 3.98 MPa, corresponding to reduced pressures between 0.27 and 0.98. The mass flux was varied between 300 kg/m²s and 2000 kg/m²s, while the local critical vapor quality ranged from highly subcooled conditions −3.43 up to 0.69. The uniformly heated tube had an inner diameter of 10 mm and heated lengths of 1 m and 3 m. The extensive experimental matrix resulted in a total of 500 CHF data points. At the onset of the boiling crisis, the wall temperature increases rapidly due to the significantly lower heat transfer capability of the vapor phase compared to the liquid phase. Under high subcritical pressure conditions, specifically at reduced pressures of above 0.8, this temperature excursion became less pronounced, particularly under dryout conditions. At the same time, the critical vapor quality marking the onset of the boiling crisis shifted toward lower values and the CHF decreased significantly as the system pressure approached the critical pressure. In experiments performed at reduced pressures of 0.95 and 0.98, CHF was in some cases observed upstream of the outlet of the heated section, a phenomenon referred to as upstream-CHF. The experimental results show that the occurrence of upstream-CHF is strongly influenced by inlet subcooling and mass flux. Based on the measured wall temperature distributions, a possible explanation for this behavior is the onset of homogeneous nucleation at a local wall temperature maximum along the heated surface. The results provide a comprehensive CHF dataset for R-134a over a wide range of operating conditions close to the critical pressure and contribute to an improved understanding of CHF behavior and the upstream-CHF phenomenon under near-critical pressure conditions.

Nomenclature

Bo	Boiling-Number [–]
C_P	Specific Heat Capacity [J/kgK]
D	Diameter [mm]
E	Statistical Error [–]
g	Gravity: 9.81 [m/s²]
G	Mass Flux [kg/m²s]
h	Enthalpy [J/kg]
h_{fg}	Heat of Vaporization [J/kg]
I	Current [A]
L	Length [mm]
$\dot{m}$	Mass Flow Rate [kg/s]
MAE	Mean Absolute Error [–]
ME	Mean Error [–]
N	Number of Datapoints [–]
P	Pressure [MPa]
P_{red}	Reduced Pressure (P/Pc) [–]
$\dot{Q}$	Heat Rate [W]
q	Heat Flux [W/m²]
$\dot{q}_{vol}$	Volumetric Heat Flux [W/m³]
RMS	Root Means Square Error [–]
s	Wall Thickness [mm]
T	Temperature [°C]
t	Time [s]
U	Voltage [V]
We	Weber-Number
x	Quality [–]
z	Relative Length [–]

✉ Nikolai Rensch
Nikolai.Rensch@kit.edu

Aurelian Florin Badea
Aurelian.Badea@kit.edu

Xu Cheng
Xu.Cheng@kit.edu

[1] Institute for Applied Thermofluidics (IATF), Karlsruhe Institute of Technology (KIT), Kaiserstraße 12 – Building 07.08, Karlsruhe 76131, Germany

Published online: 20 May 2026

Greek Symbols

Δ	Standard deviation of parameter X [unit of X]
λ	Thermal Conductivity [W/mK]
μ	Dynamic Viscosity [kg/ms]
ρ	Density [kg/m³]
σ	Surface Tension [N/m]

Subscript

c	Critical State
cor	Correlation
CHF	Critical Heat Flux
H	Hydraulic
HN	Homogeneous Nucleation
exp	Experimental
h	Heated
i	Inner
in	Inlet
j	Datapoint
l	Liquid
loss	Loss
meas	Measured
o	Outer
out	Outlet
sat	Saturation State
sub	Subcooled
TE	Thermocouple
v	Vapor
w	Wall

1 Introduction

Supercritical fluids are expected to be used more often in future high performance energy systems. During normal supercritical operating conditions, the fluid remains in a single phase and does not lead to a boiling crisis. However, during transient procedures, such as startup, shutdown or in case of an accident, the system pressure may drop below the critical point. If this happens, the system will go through high subcritical pressure conditions and may experience boiling crisis with a heat flux which is called the critical heat flux (CHF). This condition is characterized by a sudden rise in wall temperature, which can damage heating elements. CHF is therefore a key design parameter for ensuring safe operation and defining safety margins in boilers, steam generators, and other thermal power systems. It also plays an important role in setting safe operating limits for newly planned power plants [1]. The boiling crisis can be divided into two phenomena. First is the dryout which is more likely to happen in high vapor qualities, and second, the transition from nucleate boiling to film boiling, commonly referred to as Departure from Nucleate Boiling (DNB), which occurs in the low vapor quality or subcooled flow region [2, 3].

Due to the significant impact of pressure on CHF, it is important to investigate CHF in a wide range of pressure conditions, especially in the high subcritical pressure region. In this regime, even small pressure fluctuations can have a significant impact on the CHF. This sensitivity is primarily attributed to the changes in fluid properties near the critical pressure, which in turn influence both the flow behavior and the heat transfer characteristics [4–6]. For example, important fluid properties that strongly influence the CHF value include the difference between the saturated liquid and vapor enthalpy, the density difference, and the surface tension. As pressure increases, especially near the critical pressure, the latent heat of vaporization decreases significantly. As a result, less energy is required to generate vapor, so the liquid evaporates more easily, and the CHF value decreases. In addition, increasing pressure reduces the density difference between the liquid and vapor phases. This weakens the buoyancy effect and decreases vapor removal, which further contributes to lower CHF. Furthermore, surface tension decreases with increasing pressure, approaching zero at the critical pressure, which promotes the formation of a vapor film on the heated surface and reduces the thickness of the liquid film before dryout occurs.

Experimental investigations of CHF at high pressures, particularly near the critical pressure, remain relatively limited. Only a few studies have systematically examined CHF behavior under these conditions. Vijayrangan et al. [3] conducted experiments with R-134a in a 12.7 mm diameter tube at reduced pressures up to 0.98. Their results showed that, for a given mass flux, CHF decreases with increasing system pressure. In addition, the influence of mass flux becomes more pronounced at high reduced pressures (P_{red} > 0.75), where lower mass fluxes lead to significantly lower CHF values. Hong et al. [7] performed experiments with R-134a at reduced pressures up to 0.995 and reported that, near the critical pressure, CHF occurs at comparatively low heat fluxes and does not lead to the abrupt wall temperature excursions typically observed at lower pressures. Zhu et al. [8] investigated CHF with water up to a reduced pressure of 0.995 and found that dryout dominates the heat transfer deterioration in the subcritical pressure region. However, as the pressure approaches the critical pressure, the corresponding vapor qualities decrease, and the mechanism tends to shift toward DNB-type behavior. Both studies also observed a pronounced decrease in CHF as the pressure approaches the critical pressure. Furthermore, Zhu et al. reported that the dryout point shifts toward lower vapor qualities with increasing pressure. Earlier work by Nishikawa et al. [9], who conducted CHF experiments with R-22 up to a reduced

pressure of 0.96, also showed that CHF and the critical vapor quality decreases significantly as the system pressure approaches the critical pressure. Despite these contributions, experimental data on CHF behavior near the critical pressure remains limited. Consequently, further experimental investigations are required to improve the understanding and modeling of CHF phenomena in this high-pressure region.

In special cases during the CHF experiments the occurrence of a so-called upstream-CHF could be observed. In this scenario, the boiling crisis does not start at the end of the heated section, as normally expected, but rather in the middle or even near the inlet [10]. The phenomenon of upstream-CHF was first discovered in 1962 by Waters et al. [11]. During his experiments with water in a 3.66 m long uniformly heated tube with an inner diameter of 11.2 mm, such behavior was observed in both horizontally and vertically oriented flow configurations. The experimental conditions were set at a pressure of 6.9 MPa and 10.34 MPa, with very high mass fluxes of 6781 kg/m²s, and local vapor qualities at the point of the boiling crisis between 0.1 and 0.3. At lower mass fluxes, no upstream-CHF was observed.

Groeneveld et al. [12] investigated this phenomenon in more detail, conducting CHF experiments with R-12 over a wide range of mass fluxes above 4000 kg/m²s. The local vapor qualities in those experiments ranged from 0.08 to 0.45. In his study, Groeneveld also observed the occurrence of the upstream boiling crisis. He reported that the relationship between CHF and critical vapor quality changes in such a way that a local minimum appears in the corresponding curve. Since this trend can't be considered by existing CHF correlations, a reliable prediction of upstream-CHF is not possible. Additionally, it has been observed that the boiling crisis in the case of upstream-CHF propagates both downstream and, in parts, upstream [13]. Table 1 summarizes experimental studies from the literature where upstream-CHF was observed using vertically flowing tubes. The table provides details about the working fluid, pressure, mass flux, hydraulic diameter, and critical vapor quality. As indicated, this phenomenon occurs predominantly at high mass fluxes and low critical qualities. Although upstream-CHF has been observed at low mass fluxes in a few cases [10]. Overall, upstream-CHF has been addressed by only a small number of studies, and a comprehensive physical explanation of the phenomenon is still lacking.

An accurate prediction of the upstream-CHF effect and the corresponding CHF values remain challenging, as no established CHF correlations are available that can reliably predict upstream-CHF. In particular, the onset and axial location of boiling crises are not sufficiently well understood. Moreover, the spatial propagation of the abrupt temperature increase associated with upstream-CHF is highly complex, and the limited availability of experimental data hinders the development of a new, reliable correlation.

Based on the upstream-CHF behavior observed in the literature attempts were made to understand the background of this phenomenon. An explanation given by Groeneveld et al. [12, 13] refers to foam flow and its behavior. At high mass fluxes, where upstream-CHF is more likely to occur, the vapor bubbles in a foam flow tend to be smaller, resulting in a more homogenous foam layer. This leads to a maximum vapor volume fraction at the heated wall, which deteriorates the heat transfer characteristics. This leads to a boiling crisis located upstream from the end of the heated length. Since this attempt to explain upstream-CHF no further explanation and no detailed investigation were made.

To justify the use of R-134a as a model fluid for the reference fluid commonly used in thermal–hydraulic studies, namely water, it should be noted that it exhibits similar thermophysical properties and phase-change behavior. Its vapor-liquid phase boundaries in the pressure-enthalpy diagram are comparable to those of water, allowing meaningful comparisons of thermodynamic cycles and two-phase flow behavior. Moreover, the critical pressure and temperature of R-134a are significantly lower than those of water, which substantially reduces the technical requirements for experimental facilities. This simplifies facility design and operation and lowers both setup and operating costs. In addition, the lower specific heat capacity, latent heat of vaporization, and thermal conductivity of R-134a reduce the required

Table 1 Experimental investigations of the upstream-CHF phenomenon from literature

Author	Fluid	$\mathbf{P_{red}}$ [–]	P [MPa]	G [kg/m²s]	D_H [mm]	X_{CHF} [–]
Waters et al. [11]	Water	0.313 –0.469	6.9 –10.3	6781	11.2	0.1 –0.3
Bertoletti et al. [14]	Water	0.227	5.0	3900	15.0	0.13
Hassid et al. [15]	Water	0.227	5.0	2200 –3800	15.0	0.17 –0.30
Groeneveld et al. [12]	R-12	0.169 –0.363	0.7 –1.5	4100 –8100	7.8	0.08 –0.45
Merilo [16]	R-12	0.266	1.1	3400 –5410	12.6	0.10 –0.25
Merilo & Ahmad [17]	R-12	0.266	1.1	8100	5.3	0.12 – 0.20
Katto & Ashida [18]	R-12	0.484 –0.822	2.0 –3.4	2700 –7000	5.0	N/A
Yokoya et al. [19]	R-115	0.447 –0.959	1.4 –3.0	3270 –6540	5.0	0.0 –0.2

*N/A = Not available

heating and cooling power, which further decreases the operational effort.

The primary objective of the present study is to experimentally investigate the critical heat flux behavior of R-134a in a wide pressure range, especially close to the critical pressure over a wide range of operating conditions. In particular, the experiments focus on the influence of mass flux and inlet subcooling on CHF under high reduced pressure conditions. For this purpose, systematic experiments were conducted in vertically heated tubes with different heated lengths. During the experimental campaign, a boiling crisis behavior was observed, where CHF occurred significantly upstream of the outlet location. This upstream-CHF phenomenon was not initially the focus of the study but was analyzed in detail once it was identified in several experiments. The present work therefore provides both new CHF data under near-critical pressure conditions and experimental observations that contribute to a better understanding of the upstream-CHF phenomenon.

2 Experimental facility and methods

2.1 Experimental facility

The experiments of this study were carried out at the KIT Model Fluid Facility (KIMOF), a schematic overview of it is presented in Fig. 1a. The working fluid used in this study was the refrigerant R-134a. Circulation of the fluid was maintained by a coolant pump. Downstream of the pump, the fluid was preheated either via a burner or an electric flow heater, depending on the required operating conditions. For higher mass flow rates, a combination of both may be used. The mass flow rate was measured using a Coriolis flow meter, followed by the test section equipped with temperature and pressure sensors, as illustrated in Fig. 1b and described in more detail in the following section. After the test section, two heat exchangers were used to ensure the cooling of the fluid. The first heat exchanger works with a cooling tower, operating with cooled water and the second one works with a cooling machine. Both together have a

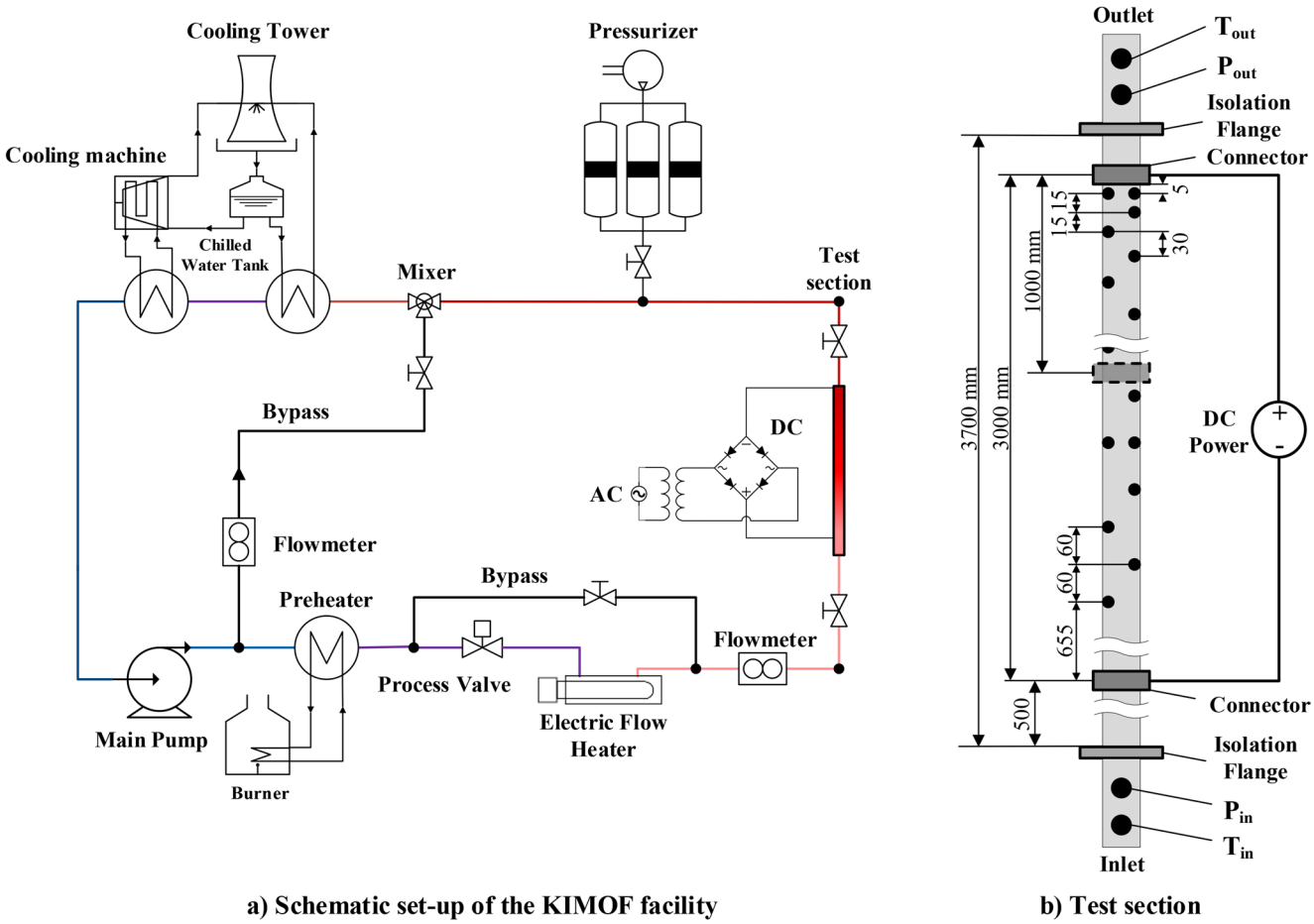

Fig. 1 Schematic set-up of the KIMOF facility and the test section with the corresponding measurement devices

total cooling power of 800 W and can ensure a minimum fluid temperature of −5 °C. To adjust and regulate the pressure in the system, a pressurizer was used, which operates with oil on the hydraulic side. During the operation of the facility, a control system ensures the coordinated operation of the entire setup. The data of the control system as well as four data loggers provide all relevant measurement parameters, which were further used and displayed by LabVIEW.

2.2 Test section

The round test tube had a total length of 3700 mm with an outer diameter of 12.7 mm and an inner diameter of 10 mm and was installed vertically. The test tube is made of Alloy 625 which is a nickel-chromium-molybdenum-niobium alloy and can be used for temperature applications up to 1050 °C. Furthermore, the material exhibits excellent resistance to a wide range of corrosive media [20]. To provide electrical heating to the test section, two current connectors were used. These connectors defined a heated length of 3 m during the first experimental session, which was subsequently reduced to 1 m for the second session. Two isolation flanges were used to avoid damage to the measurement devices and other components due to the electrical supply of the test section. The test section was heated by uniform direct current (DC) provided by a transformer. In total 60 type-T thermocouples (black dots in Fig. 1b) with a diameter of 1 mm were alternately mounted along the outer side of the test section. To provide electrical insulation an initial layer of Hi-Bond HB830 tape with a polyimide layer thickness of 25 µm and a silicone adhesive layer thickness of 45 µm was attached to the tube. A second layer secured the sensor in place. The first thermocouple was positioned 655 mm above the lower DC connector. In the lower part of the section, the longitudinal distance between each thermocouple was 60 mm. In the upper part, the distance is reduced to 30 mm, while the last four thermocouples were spaced 15 mm apart. The final thermocouples were located 5 mm below the upper DC connector at the end of the heated section. The reason for the reduction of the axial spacing was to achieve a higher spatial resolution in the region where the boiling crisis was expected. The temperature and the pressure of the fluid at the inlet and outlet were measured with a mineral insulated type-T thermocouple and a pressure transmitter of type PXM35, respectively. To ensure a fully developed hydrodynamic flow at the beginning of the heated section, an unheated inlet length was provided. The distance between the entrance of the tube and the first current connector was either 500 or 2500 mm, which corresponds to inlet length-to-diameter ratios (L/D_H) of 50 and 250, respectively. To reduce the heat loss, the test tube was surrounded by two layers of mineral wool with a total thickness of 50 mm and a thermal conductivity of 0.035 W/mK.

2.3 Experimental procedure and matrix

The CHF experiments were carried out at constant pressure, inlet temperature and mass flux as quasi-steady-state experiments. After setting the mentioned parameters, starting with the lowest subcooling temperature, the heat flux was increased until one thermocouple suddenly detected a steep temperature jump of at least 10 °C. The increase of the heat flux was between 0.5 and 2.0 kW/m² for every step, depending on the operating parameters, with larger steps at higher heat fluxes. This stepwise increase was imposed by the transformer characteristics. After each step, all parameters have to reach a steady state condition. Each measurement was recorded at 5 Hz. This sampling rate was sufficient to identify the onset of the boiling crisis and trigger the safety shutdown, while the quasi-steady-state approach ensured that the CHF value itself was determined by the power increment rather than the temporal resolution of the transient. After the CHF was successfully measured a higher subcooling temperature was set and the procedure started again. During one measurement, several parameters such as the inlet temperature, the mass flux and the pressure must be kept within a certain range. The tolerance range of the inlet temperature was kept within $\pm\ 0.5\ ^\circ\mathrm{C}$ and the pressure within $\pm\ 0.03\ \mathrm{MPa}$. For the mass flux a deviation of 2% was kept. To prevent thermal decomposition of the refrigerant R-134a, the safety shutdown was set to a maximum wall temperature of 240 °C, as higher temperatures could alter the fluid and thus the operating conditions of the facility. The experimental matrix is shown in Table 2 which covers a wide range of pressures up to an outlet pressure near the critical point. The reduced pressure P_{red} was calculated using the measured outlet pressure, as the boiling

Table 2 Matrix for the experiments with the 3 m and 1 m heated length

$\mathbf{L_h}$ [mm]	$\mathbf{P_{red}}$ [-]	P [MPa]	$\Delta\,\mathbf{T_{sub}}$ [°C]	G [kg/m²s]
3000	0.70	2.84	[5.0; 65.0]	300, 600, 1000, 1500
	0.80	3.25	[5.0; 75.0]	
	0.90	3.65	[5.0; 80.0]	
	0.95	3.86	[5.0; 83.0]	
	0.98	3.98	[5.0; 85.0]	
1000	0.27	1.10	[15.0; 38.0]	300, 600, 1000, 1500, 2000
	0.42	1.70	[13.5; 55.5]	
	0.70	2.84	[23.6; 78.6]	
	0.80	3.25	[30.1; 85.1]	
	0.90	3.65	[10.8; 90.8]	
	0.95	3.86	[21.6; 93.6]	
	0.98	3.98	[19.1; 96.1]	

crisis generally occurred at the end of the heated section. Besides that, a wide range of mass flux conditions were chosen, which covers the limits of the KIMOF facility. The inlet subcooling ΔT_{sub} represents the minimum and maximum values selected for the experiments. The step size between these values ranged between 2.5 and 10 °C.

2.4 Data reduction

The important data to investigate the critical heat flux will be shown in this subsection. The critical heat flux q_{CHF} itself was calculated by Eq. (1).

$$q_{CHF} = \frac{UI - \dot{Q}_{loss}}{\pi\, L_h D_i} \tag{1}$$

U represents the voltage and I the current, the product of both corresponds to the electrical power. $\dot{Q}_{loss}$ describes the heat loss of the test section. Both are divided by the area of the heated wall with L_h as the total heated length and D_i as the inner diameter of the test tube.

The corresponding critical vapor quality x_{CHF} is calculated by the following Eq. (2).

$$x_{CHF} = \frac{h_{CHF} - h_l}{h_v - h_l} \tag{2}$$

in which h_l and h_v are the enthalpies at liquid and vapor saturation calculated with the measured outlet pressure, respectively. h_{CHF} represents the enthalpy at the point where boiling crisis occurs in the heated tube and can be calculated by Eq. (3). Where the inlet enthalpy at the entrance of the test tube is h_{in} which is calculated by the inlet pressure and temperature, and G is the mass flux. L_{CHF} represents the heated length to the thermocouple which detects the boiling crisis.

$$h_{CHF}\,(L_{CHF}) = h_{in} + \frac{4 q_{CHF}}{G D_i} L_{CHF} \tag{3}$$

In the discussion section, the position of the thermocouples is used and represented by the relative heated length, which can be calculated using Eq. (4) by dividing the corresponding thermocouple position L_{TE} by the total heated length L_h.

$$z = \frac{L_{TE}}{L_h} \tag{4}$$

To calculate the inner wall temperature, the one-dimensional, stationary Fourier heat conduction equation was used. The final derivation to calculate the inner wall temperature $T_{w,i}$ is shown in Eq. (5).

$$T_{w,i} = T_{w,o} + \frac{\dot{q}_{vol}}{16\lambda_w}\left(D_o^2 - D_i^2\right) + \frac{D_o}{2\lambda_w}\left(\frac{\dot{q}_{vol}}{4} D_o - q_{loss}\right)\ln\left(\frac{D_i}{D_o}\right) \tag{5}$$

D_o describes the outer diameter of the tube, $T_{w,o}$ the measured outer wall temperature and λ_w represents the thermal conductivity of the wall. The volumetric heat flux $\dot{q}_{vol}$ and the loss of heat flux q_{loss} are calculated by Eqs. (6) and (7), respectively.

$$q_{loss} = \frac{\dot{Q}_{loss}}{\pi\, L_h D_o} \tag{6}$$

$$\dot{q}_{vol} = \frac{4UI}{\pi\, L_h\,(D_o^2 - D_i^2)} \tag{7}$$

The heat losses $\dot{Q}_{loss}$ were determined experimentally using a vacuum-sealed test section in order to eliminate convective heat transfer. Electrical heating power was applied in several steps, and the corresponding outer wall temperatures were recorded. Based on these measurements, a correlation was fitted to describe the heat loss as a function of the temperature difference between the outer wall $T_{w,o}$ and the environment temperature T_u. The resulting correlations for both heated lengths were obtained using a least-squares regression with a second-order polynomial function and are given by Eq. (8).

$$\dot{Q}_{loss} = \begin{cases} 5.46 \bullet 10^{-4}(T_{w,o} - T_u)^2 + 0.314\,(T_{w,o} - T_u) - 0.212 & ; \quad L_h = 3\,m \\ 1.87 \bullet 10^{-4}(T_{w,o} - T_u)^2 + 0.103\,(T_{w,o} - T_u) - 0.017 & ; \quad L_h = 1\,m \end{cases} \tag{8}$$

The corresponding experimental data and fitted curves are shown in Fig. 2. As can be seen, the fitted correlations show good agreement with the experimental data and were used to correct the electrical heating power during the CHF experiments.

2.5 Measurement uncertainties

During the CHF experiments the heat flux, outer wall temperature, mass flux, inlet as well as outlet pressure and temperature were measured. The corresponding uncertainties of the test tube geometry and instrumentations are shown in Table 3. In addition, the standard deviation and therefore the uncertainty of the CHF value $\Delta_{q_{CHF}}$ and the critical vapor quality $\Delta_{x_{CHF}}$ was calculated using error propagation, as shown for q_{CHF} in Eq. (9) and indicated in the following figures. The overall average uncertainty of the CHF values was calculated to be 3.5% and the average standard deviation for the critical vapor quality is 0.047 with a minimum

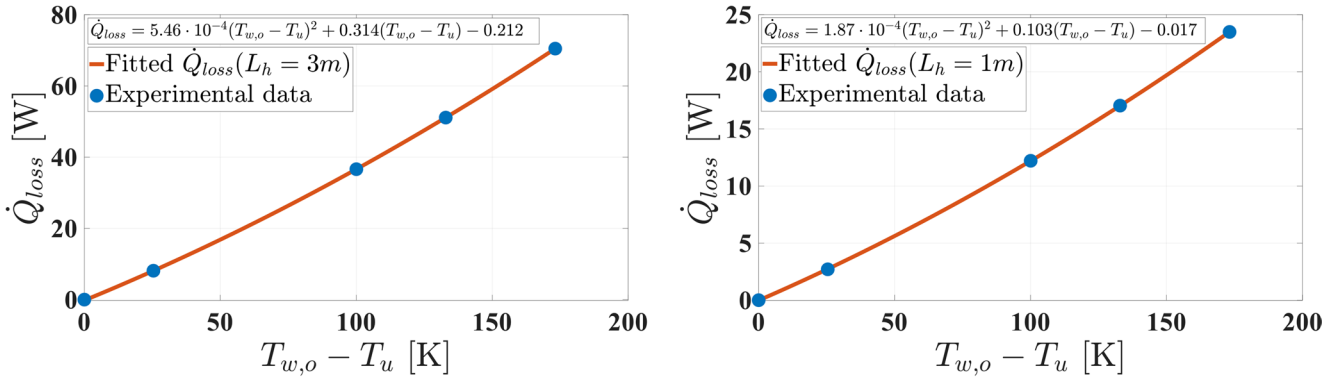

a) Heat loss determination for the 3 m heated length

b) Heat loss determination for the 1 m heated length

Fig. 2 Determined heat loss as a function of the temperature difference between the outer wall and environment temperature

Table 3 Parameters and manufacturing uncertainties

T_{in} & T_{out}	$T_{w,i}$	P_{in} & P_{out}	$\dot{m}$	U	I	D_o	s	L_h
max. 0.7 °C	max. 0.66 °C	0.25%	0.05%	0.03%	1.5%	0.05 mm	10%	0.5 mm

of 0.013 and a maximum of 0.139. The uncertainty associated with the heat loss correction was included in the overall uncertainty analysis. The average standard deviation of the heat loss is $\Delta_{\dot{Q}_{loss}} = 0.35$ W, which corresponds to a relative uncertainty of only 0.008% with respect to the total applied heat. The higher standard deviations of the critical vapor qualities are related to operating points near the critical pressure, where the heat of vaporization strongly decreases with increasing pressure. All thermodynamic properties of R-134a were calculated using the NIST Reference Fluid Thermodynamic and Transport Properties Database (REFPROP), version 10.0 [21]. Moreover, to check the installed instrumentations, heat balance tests were conducted under single-phase flow conditions. During the tests, the enthalpy increase of the fluid was determined in two independent ways. First, it was calculated from the applied heating power and mass flow using energy balance. Second, the enthalpy difference was obtained from the measured inlet and outlet thermodynamic states using NIST property data. The mean deviation between both methods was 3.52% before the experimental session and 2.52% afterwards.

$$\Delta_{q_{CHF}} = \sqrt{\left(\frac{\partial q_{CHF}}{\partial U}\Delta_U\right)^2 + \left(\frac{\partial q_{CHF}}{\partial I}\Delta_I\right)^2 + \left(\frac{\partial q_{CHF}}{\partial \dot{Q}_{loss}}\Delta_{\dot{Q}_{loss}}\right)^2 + \left(\frac{\partial q_{CHF}}{\partial L_h}\Delta_{L_h}\right)^2 + \left(\frac{\partial q_{CHF}}{\partial D_i}\Delta_{D_i}\right)^2} \quad (9)$$

To check the reproducibility of the obtained data, experiments were repeated after around 2 months. Overall, the test runs showed that the experiments can be reproduced well. The mean relative absolute deviations of all CHF values were calculated to be 1.91%. Some of the cases, indicated by the letters A-H, are represented in Fig. 3, which support the good agreement between the first experiments and the repeated once.

Due to temperature gradients along the heated tube, axial heat conduction in the streamwise direction was calculated. The magnitude of this axial heat transfer increases with increasing temperature differences over short axial distances. Therefore, the axial heat conduction between adjacent tube segments was calculated and compared with the applied heating power of each segment. For the experiments in this study, the maximum contribution of axial heat conduction within a single segment was found to be 0.69% of the local heating power, corresponding to approximately 0.16 W. These results indicate that axial heat conduction is negligible under the present CHF experimental conditions. The small contribution of the axial heat conduction further supports the validity of the one-dimensional heat conduction assumption for Eq. (5).

3 Experimental results and discussion

This section presents the experimental results of the CHF investigations, especially near the critical pressure. The effects of critical vapor quality, heated length, mass flux, and system pressure on the CHF are analyzed. To calculate the fluid properties at CHF the outlet pressure was used.

3.1 Influence of heated length on CHF

By systematically varying the heated length while keeping the mass flux and the pressure constant, an approximately linear relationship between CHF and the critical vapor quality is observed. This behavior can be directly explained by the energy balance along the heated section. For a given

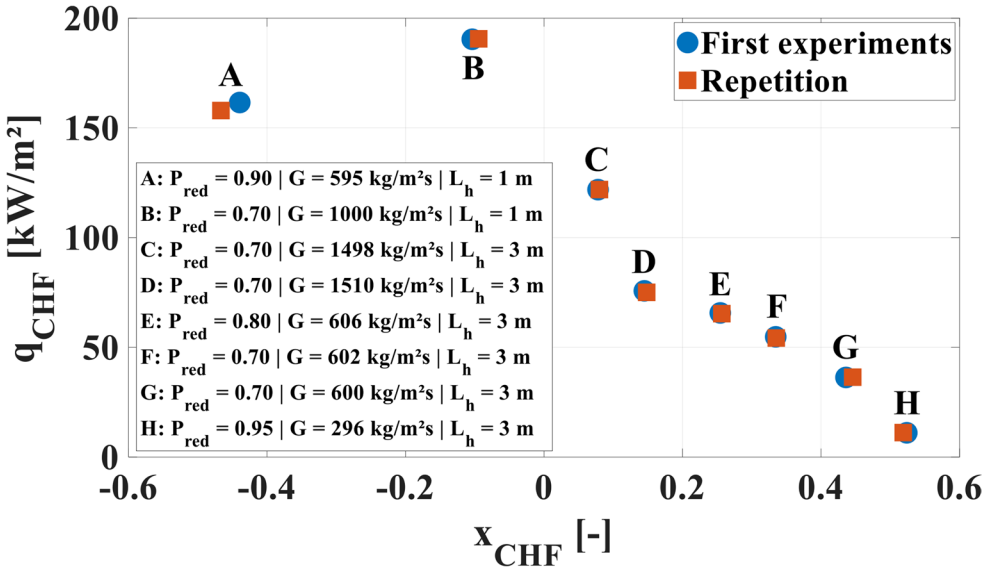

Fig. 3 Repeatability of CHF experiments

heated length and critical heat flux, the total energy added along the section has to match the difference between the inlet enthalpy and the critical enthalpy, according to Eq. (3). Consequently, shortening the heated length reduces the energy supplied along the section, requiring a higher inlet enthalpy to reach the same critical enthalpy. Conversely, increasing the heated length allows a lower inlet enthalpy for the same critical enthalpy. In addition, if the critical enthalpy itself changes, the critical heat flux must adjust proportionally to satisfy the energy balance, leading to a corresponding increase or decrease in CHF. This combined effect of varying both heated length and critical enthalpy results in a linear extension of the CHF vs. critical vapor quality curves. The curves corresponding to larger heated lengths are systematically shifted and extended, producing the extensions of the curves for two different heated lengths, shown in Fig. 4a and 4b. This behavior is independent of the pressure and mass flux as can be seen in the figures.

In addition, the figures show the general trend of the increasing CHF with decreasing critical vapor quality. This can also be explained by the energy balance. As the critical vapor quality decreases, the liquid volume fraction increases. Since the liquid can absorb and remove more heat before dryout occurs, the wall can sustain a higher heat flux before reaching the critical heat flux.

3.2 Influence of mass flux on CHF

If the CHF is considered as a function of the local critical vapor quality for different mass fluxes, Fig. 5a and b show that the influence of mass flux depends strongly on the critical vapor qualities. At strongly negative local vapor qualities, as shown in Fig. 5a, the CHF generally increases with increasing mass flux. This behavior can be attributed to the higher fluid velocity and the resulting enhancement of convective heat transfer. In addition, the increased velocity promotes turbulence, which facilitates the detachment and removal of vapor bubbles from the heated wall into the bulk flow during the boiling process [22]. Efficient removal of vapor bubbles in this regime is important, since

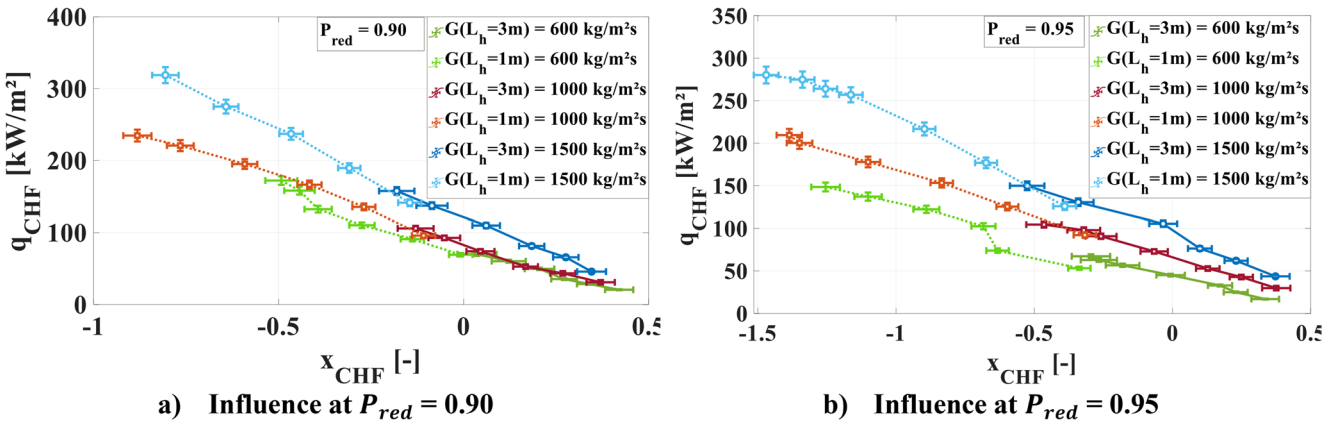

a) Influence at $P_{red} = 0.90$ b) Influence at $P_{red} = 0.95$

Fig. 4 Influence of heated length on CHF and critical vapor quality at different reduced pressures and mass fluxes

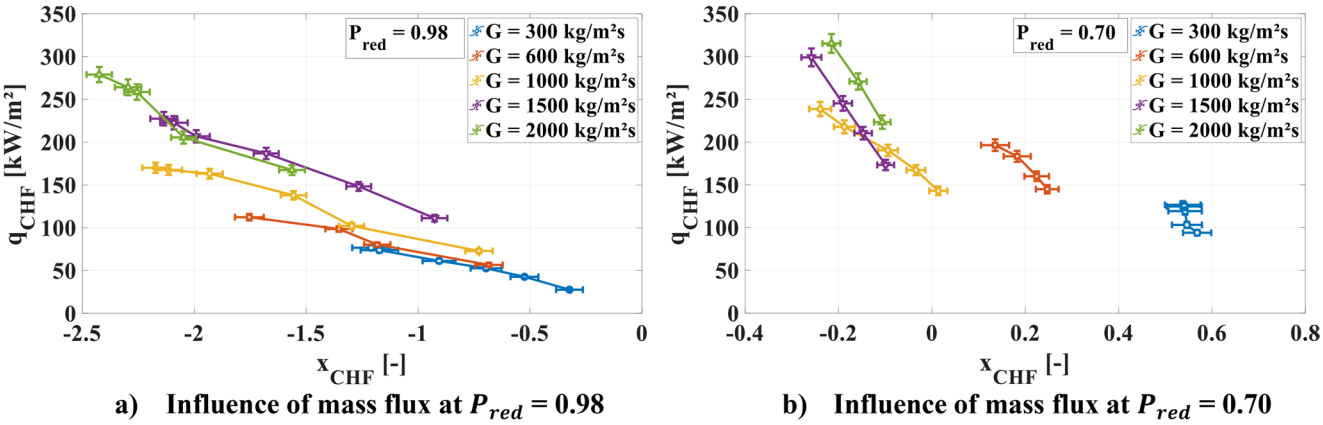

Fig. 5 Influence of mass flux on CHF at different reduced pressures for a heated length of 1 m

insufficient bubble detachment can lead to the rapid formation of an insulating vapor layer at the heated surface. Under these conditions, CHF behavior is typically associated with DNB-type mechanisms. In contrast, Fig. 5b shows that at higher or slightly positive critical vapor qualities the influence of mass flux on CHF becomes weaker as the mass flux increases. This behavior is commonly referred to as the inverse mass flux effect [2]. The reduced sensitivity of CHF to mass flux under these conditions is often associated with dryout-type mechanisms. With increasing mass flux, the interaction between the phases in the near-wall region becomes stronger, which can enhance the removal of liquid from the wall region. Consequently, the liquid supply available for cooling the heated surface may decrease, which can promote the earlier onset of conditions leading to CHF. Similar tendencies have been discussed in the literature, for example by Pioro et al. [23]. It should be noted that a strict distinction between DNB and dryout is difficult under the high-pressure conditions investigated in this study. As the system pressure approaches the critical pressure, the thermophysical properties of the fluid change drastically and the heat of vaporization decreases significantly. As a consequence, the calculated critical vapor quality becomes highly sensitive to the heat of vaporization and may therefore result in very small or strongly negative values. Under such conditions, classical vapor quality criteria that are commonly used to distinguish between DNB and dryout become less reliable.

In the present experiments, the distinction between DNB-type and dryout-type behavior was based on the temporal characteristics of the wall temperature excursion at the CHF point. Under dryout-type conditions, which were predominantly observed at higher or slightly positive vapor qualities, the wall temperature increased gradually, allowing the system to approach a quasi-steady wall temperature level below the safety limit of 240 °C. This is attributed to the continued contribution of convective heat transfer in the post-CHF region, where a vapor core with entrained liquid droplets maintains partial heat removal from the wall even after depletion of the liquid film. In contrast, events occurring at strongly negative vapor qualities exhibited a rapid and pronounced wall temperature rise that consistently triggered the safety shutdown, preventing the system from reaching a quasi-steady state condition. This behavior is characteristic of DNB-type conditions, where a continuous vapor layer forms between the heated wall and the liquid core. Since heat transfer is then governed primarily by conduction through this vapor layer, whose thermal conductivity is substantially lower than that of the liquid phase, the heat removal capability is strongly reduced, resulting in the observed abrupt temperature excursion. It should be emphasized that this interpretation relies on the temporal development and stability of the temperature signal rather than on absolute wall temperature values alone and therefore remains valid within the thermocouple measurement uncertainty discussed in Sect. 2.5.

3.3 Influence of pressure on CHF

As described in the introduction, the pressure has a significant influence on the CHF, which strongly depends on the fluid properties. Higher pressures lead to lower CHF values. This is because the enthalpy of vaporization, density difference, and surface tension decrease with increasing pressure. Conversely, increasing pressure causes an increase in the specific heat capacity and thermal conductivity, which contributes to an increase in CHF. Thus, a combination of several factors interacts with each other, which influence the CHF depending on the flow quality and pressure [24]. Mudawar & Bowers [25] as well as Celata & Mariani [26] reported that early studies showed the CHF initially increases with pressure in the low-pressure range, although sometimes only a very small pressure effect was observed. However, after reaching a

pressure related maximum, the CHF decreases with further pressure increase. A similar behavior was observed in the experiments conducted in this study, as can be seen in Fig. 6. While at low pressures the influence of pressure on the CHF is relatively small, the CHF decreases more significantly at higher pressures. This decrease becomes steeper as the pressure approaches the critical pressure. Once the reduced pressure reaches unity, the boiling crisis behavior disappears, and the CHF drops to zero [27]. As the system pressure increases, the CHF values decrease, which, as previously mentioned, is related to the strongly changing enthalpy of vaporization, density difference, and surface tension. The closer the pressure approaches the critical pressure, the more pronounced this effect becomes.

The relatively large variation of CHF in a narrow range of critical vapor qualities observed in the region of low reduced pressure and comparatively high critical vapor qualities can mainly be attributed to the scaling of the diagram as well as the strong influence of pressure in the high pressure region. As the system pressure approaches the critical pressure, the heat of vaporization decreases significantly. Consequently, even small variations in operating conditions can lead to relatively large changes in critical vapor quality. In comparison, the CHF characteristic appears disproportionately steep at lower pressures on the same scale. In addition, the observed behavior may be related to the so-called limiting critical quality. Near this condition, the q_{CHF} vs. x_{CHF} curve is known to exhibit a sharp decrease, which in some cases can appear nearly vertical. Since the present experimental campaign was not specifically designed to investigate this phenomenon and the available data in this region are limited, a detailed analysis of this behavior is beyond the scope of the present work. More detailed discussions of the limiting critical quality can be found in the literature, for example in the work of Pioro et al. [28].

3.4 Comparison of experimental results with existing CHF correlations

In this subsection, two established CHF correlations are used to predict the experimental CHF results obtained in the present study. The first correlation is the local condition correlation (LCC) developed by Shah [29], while the second is the correlation proposed by Song [30]. Both correlations are formulated in dimensionless form and were evaluated with CHF data of different fluids, which is why the correlations are applicable to a wide range of fluids. The corresponding equations are provided in Appendix A1 and A2.

Table 4 summarizes the validity ranges of the Shah and Song correlation. As can be seen, both correlations cover a broad pressure range, including conditions close to the critical pressure. Furthermore, they are applicable over wide ranges of mass flux and critical vapor quality, extending to very low negative qualities.

The predicted CHF values for all experimental data points at the seven investigated pressure conditions are

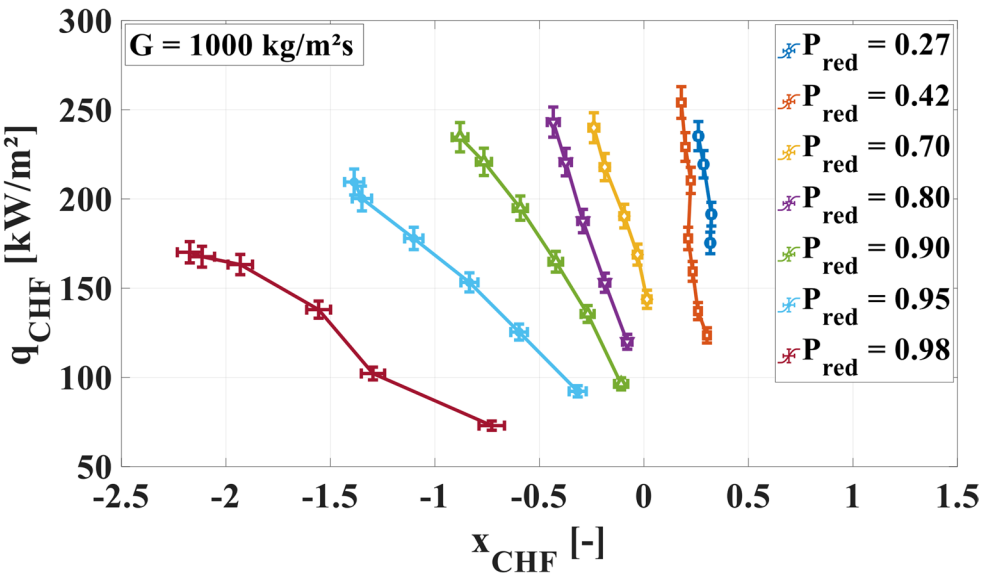

Fig. 6 Influence of system pressure on CHF for a heated length of 3 m

Table 4 Validity range of the Shah and Song correlation for predicting CHF

Correlation	D_H [mm]	P_{red} [-]	G [kg/m²s]	q_{CHF} [kW/m²]	x_{CHF} [-]	L_{CHF}/D_H [-]
Shah [29]	[0.32; 37.8]	[0.0014; 0.96]	[4; 29 051]	[0.11; 45 000]	[−2.7; 1.0]	[1.3; 940]
Song [30]	[1.9; 24.7]	[0.7; 0.97]	[121; 10 440]	[18; 7770]	[−1.77; 0.96]	-

shown in Fig. 7. The statistical indicators used to evaluate the correlations include the mean error (ME), the mean absolute error (MAE), and the root mean square error (RMS), which are also reported in the figures. The error for each data point j is calculated according to equation A3 using the predicted CHF value $q_{CHF_{j,cor}}$ and the measured CHF value $q_{CHF_{j,meas}}$ from the experiments. The definitions of the statistical parameters are provided in Appendix A4–A6. The results obtained using the Shah correlation Fig. 7a show a general overprediction of the experimental CHF values, with a mean error of 47%. Most of this overprediction occurs at higher reduced pressures above $P_{red} = 0.7$. The RMS value of 86.8% indicates that several predicted data points deviate significantly from the experimental results, particularly for lower CHF values where the correlation shows limited predictive capability. In comparison, the Song correlation Fig. 7b provides improved agreement with the experimental data. Overall, the correlation tends to underpredict the measured CHF values with a mean error of 19.3%. The RMS value of 37.7% indicates a substantially smaller scatter compared to the Shah correlation. However, for both correlations it can be observed that the prediction accuracy decreases at higher reduced pressures, where CHF values are generally lower.

4 Upstream-CHF

In the present study, upstream-CHF was primarily observed in the 1 m test section at high mass fluxes, although it also occurred at 300 $\mathrm{kg/m^2s}$ in some cases. In contrast, no upstream-CHF was detected with a heated length of 3 m. An overview of the parameters under which this phenomenon occurred is provided in Table 5. It is evident that the effect was mainly observed at pressures near the critical point. The parameter N_{exp} indicates the number of experiments in which upstream-CHF was detected. A closer look at the

Table 5 Parameter range of the upstream-CHF experiments in $L_h = 1$m

P_{red} [-]	G [kg/m²s]	x_{in} [-]	x_{CHF} [-]	q_{CHF} [kW/m²]	N_{exp} [-]
0.95	1000 – 2000	[-3.88; -3.25]	[-1.97; -1.47]	210.6 – 313.1	6
0.98	300 – 2000	[-10.53; -4.08]	[-3.19; -1.31]	84.2 – 311.2	34

operating conditions shows that this phenomenon tends to occur with strong inlet subcooling and generally high mass fluxes, consistent with the investigations by Groeneveld [31]. As indicated in Table 5, the occurrence of upstream-CHF relative to the total number of experiments is low for the present dataset, suggesting that it is restricted to a narrow range of operating conditions. In the present study, the term upstream-CHF is used to describe CHF events that occur upstream, before the end of the heated length where CHF is typically expected under conventional conditions. Upstream-CHF was observed within a relative heated length of $0.665 \leq z \leq 0.965$. It should be noted that this definition does not imply that CHF occurs near the inlet or middle of the heated section, but rather at any axial position upstream of the end of the heated length. The reason why upstream-CHF was not observed in the experiments with a heated length of 3 m is that the required extreme thermal–hydraulic conditions could not be achieved in this configuration. Owing to the very low inlet vapor quality, substantially higher heat fluxes are required in the 1 m heated tube to reach the boiling crisis compared with the 3 m test section. As a consequence, the bulk flow in the shorter tube remains strongly subcooled over a larger portion of the heated length, particularly at high mass fluxes.

Under these conditions, boiling in the core flow is suppressed while the wall temperature can increase significantly, allowing more extreme local thermodynamic states to be reached. In the 3 m heated tube, however, the boiling crisis occurred at lower heat fluxes and higher critical vapor qualities. Furthermore, it was not possible to reduce the inlet

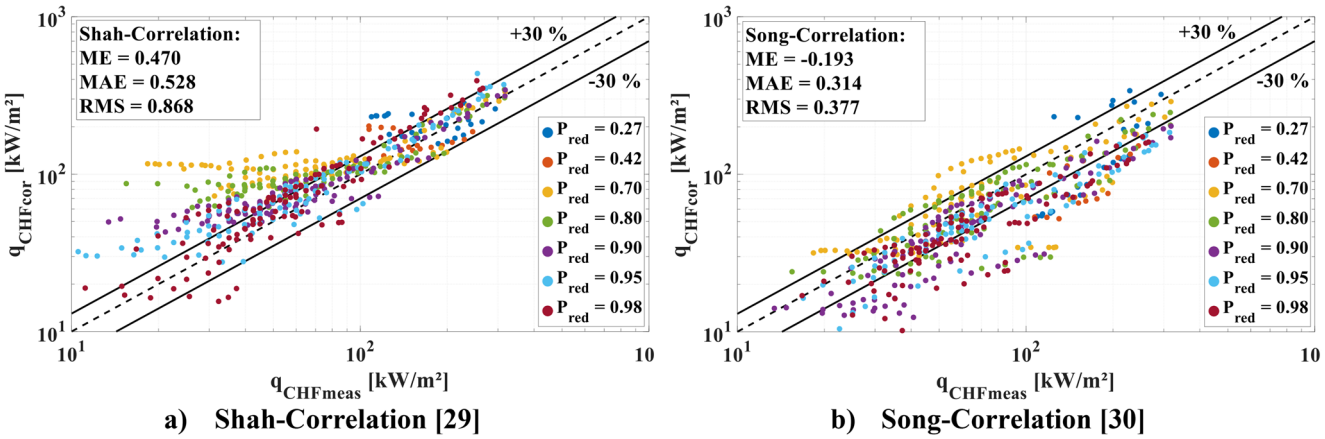

Fig. 7 Experimental CHF $q_{CHF_{meas}}$ compared with CHF predicted by the correlations $q_{CHF_{cor}}$

temperature sufficiently to reproduce the strongly subcooled conditions present in the upstream-CHF experiments. As a result, the extreme local conditions required for upstream-CHF could not be achieved in the longer test section.

An example of an instantaneous wall temperature profile shortly after the onset of the boiling crisis, in which the upstream-CHF phenomenon was observed, is shown in Fig. 8a. For comparison, Fig. 8b presents an experiment where the boiling crisis occurred at the end of the heated length. During the experiments it was carefully checked if the system parameters show fluctuations. The flow parameters remained stable throughout the tests and did not have oscillations that could have triggered the upstream-CHF effect. That such oscillations do not contribute to the onset of upstream-CHF has also been confirmed in earlier studies [10, 11]. Upstream-CHF is often followed by sudden temperature rise in its surroundings, until the boiling crisis eventually reaches the end of the heated length [12]. This behavior has also been described in the literature [10] and is sometimes referred to as a 'distributed boiling crisis' [17]

4.1 Critical heat flux vs. critical vapor quality

As reported and described by Groeneveld [13] and Kitto [10], a local minimum can occur in the trend between CHF and the critical vapor quality. Other researchers, such as Merilo [16], observed a more horizontal trend within the curve. In the present study, both types of trends were identified. For example, Fig. 9a shows the relationship between CHF and critical vapor quality at high mass flux conditions with a distinct local minimum. This minimum is attributed to the occurrence of upstream-CHF. When the boiling crisis occurred upstream, the resulting CHF values were in some cases significantly lower than expected. Similar behavior has been reported in the literature and is associated with the local minimum in the CHF vs. critical vapor quality curve described by Groeneveld and Kitto. As the critical vapor quality increases, the CHF initially decreases. However, once the boiling crisis occurs again at the end of the heated section, the CHF increases before decreasing again with a negative gradient as the critical vapor quality continues to

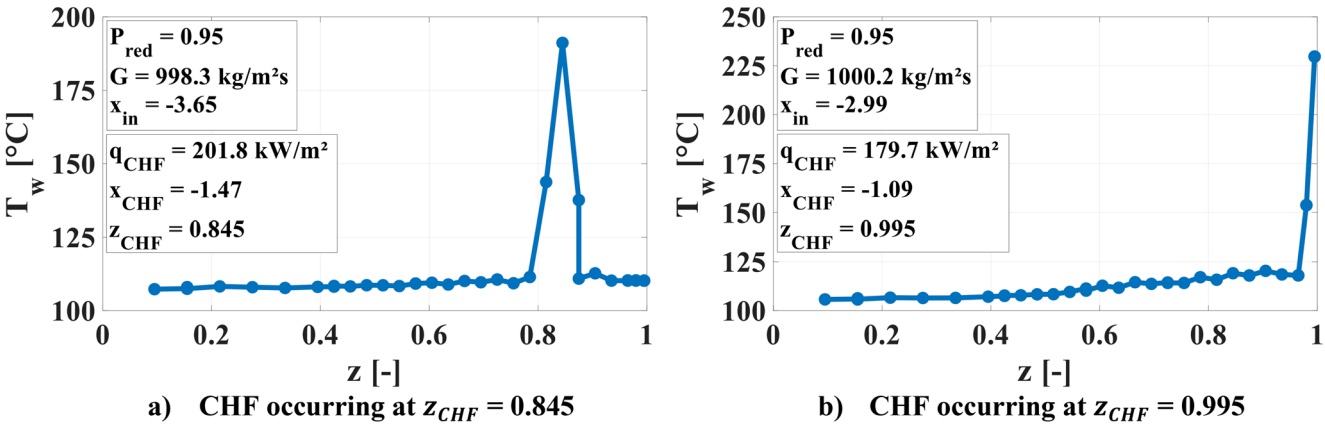

Fig. 8 Axial temperature profiles for CHF experiments with a boiling crisis occurring upstream (**a**) and at the end (**b**) of the heated length for a selected time step

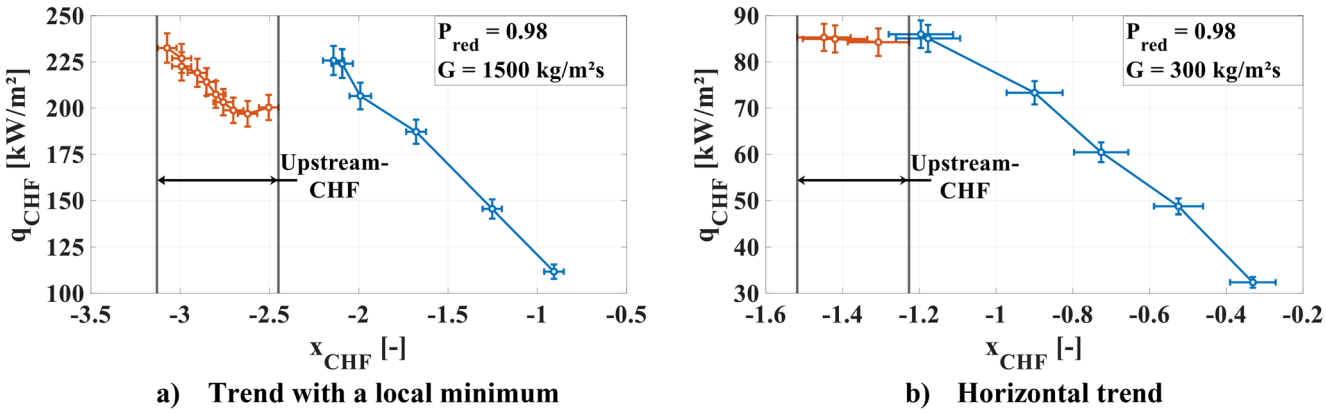

Fig. 9 CHF vs. critical vapor quality trend at a reduced pressure of $P_{red} = 0.98$ and different mass fluxes

rise. This behavior reflects the transition from upstream-CHF to conventional CHF at the outlet of the heated section. Another example is shown in Fig. 9b for low mass flux conditions, where the CHF remained nearly constant across increasing critical vapor qualities as long as the boiling crisis occurred upstream. As soon as the boiling crisis occurred again at the end of the heated length, the CHF began to decrease as the critical vapor quality increased.

It should be noted that the CHF location corresponding to the upstream-CHF data points shown in Fig. 9a and 9b can be identified from Fig. 12, where the axial CHF position along the heated length is plotted together with the corresponding x_{CHF} values.

4.2 Development of the boiling crisis under upstream-CHF conditions

This subsection illustrates the progression of the boiling crisis under upstream-CHF conditions. As mentioned before, the boiling crisis can spread to varying degrees around the initial starting point of upstream-CHF. Figure 10a shows this development by displaying the wall temperature profile as a function of the relative heated length z at different time steps. At $t=924$ s, the onset of the boiling crisis can be identified at a relative height of $z=0.845$, indicated by the blue curve showing a small temperature peak. As time progresses, the wall temperature at $z=0.845$ continues to rise. In addition, the thermocouples located near this position also begin to detect increased temperatures, showing the spread of the boiling crisis along the heated surface. Figure 10b further illustrates the temporal evolution of this process. The temperature rise at $z=0.845$ is shown by the light blue curve, while the surrounding thermocouples show a delayed temperature rise. This indicates that the boiling crisis initially spreads downstream, as seen with the green ($z=0.875$) and the purple ($z=0.905$) curve, and then spreads upstream, as shown by the pink ($z=0.815$) and dark blue ($z=0.785$) curves. It should be emphasized that the heat flux remains constant throughout the upstream-CHF process, which confirms that the observed temperature increase is not caused by an increase of power. Compared to the sharp temperature excursions typically observed in conventional CHF experiments, where the boiling crisis occurs near the end of the heated length, the wall temperature rise under upstream-CHF conditions develops more gradually. This observation aligns with findings from earlier studies, such as those by Waters et al. [11] and Kitto et al. [10], and can be observed at the corresponding times indicated in Fig. 10. It took approximately 48 s for the wall temperature to reach a maximum value of about 200 °C. The spreading of the boiling crisis to neighboring locations is mainly attributed to the decreasing local heat transfer once a vapor layer forms at the heated surface. Under these conditions, the wall must dissipate the same imposed heat flux with a significantly reduced heat transfer coefficient, which leads to a progressive increase in wall temperature at adjacent locations. In addition, axial heat conduction within the tube wall may contribute to the delayed temperature increase observed at neighboring thermocouple positions and therefore support the propagation of the boiling crisis along the heated surface.

To verify the reproducibility of the upstream-CHF experiments, a selection of tests was repeated approximately one month after the first experiments. During the repetitions, it became apparent that this phenomenon is highly sensitive and, in some cases, difficult to replicate. The ability to reproduce the behavior depends on how accurate the experimental parameters in the repeated experiments can be matched to those of the first experiments. Since the experiments were conducted close to the critical pressure, even small pressure deviations are expected to lead to noticeable discrepancies due to the significant impact of minor changes on the fluid properties. The inlet temperatures of each upstream-CHF experiments in one session were also very close to each other. The step size was only 2.5 °C. As a result, even small deviations in inlet temperature can lead to differences in CHF and critical vapor quality. An analysis

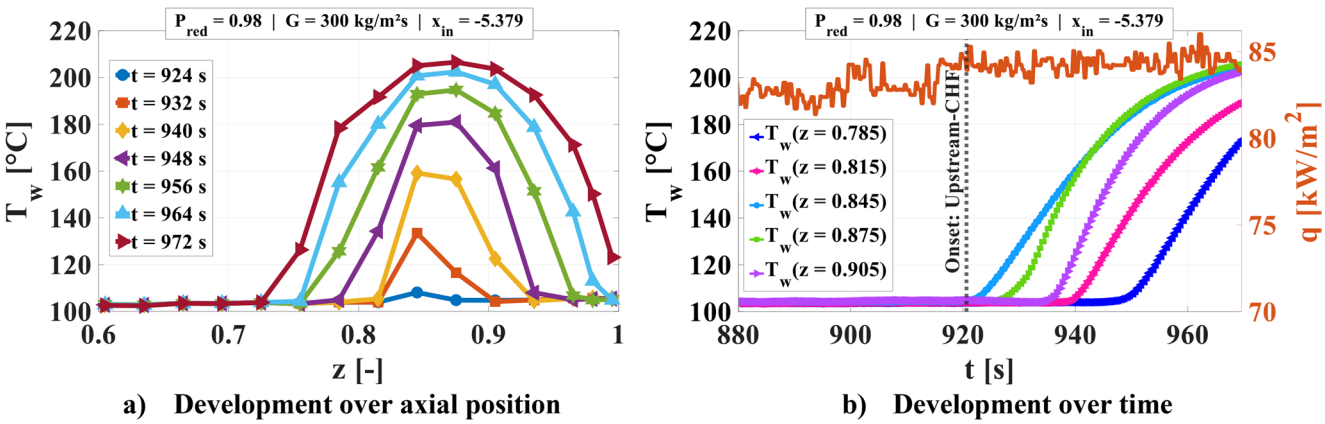

Fig. 10 Development of the boiling crisis under upstream-CHF conditions

of the repeated data provides the mean absolute errors of the upstream-CHF to be 2.58%.

It was also essential to verify whether the axial positions at which upstream-CHF occurs are reproducible. Figure 11 presents an example demonstrating this reproducibility. It is clearly observable that the temporal evolution during upstream-CHF is identical in both cases. For instance, in both the first experiment Fig. 11a and the repeated experiment Fig. 11b, the boiling crisis begins at a relative heated length of $z=0.845$. Almost simultaneously, the temperature rise spreads to the two thermocouples located upstream ($z=0.815$ and $z=0.785$) as well as to the downstream thermocouple ($z=0.875$). The sequence of temperature rises follows the same pattern in both experiments. This reproducibility is always given as long as the CHF value and the critical vapor quality match well between the first and the repeated experiments carried out under upstream-CHF conditions.

4.3 Factors influencing the position of upstream-CHF

This part of the work analyzes the factors that influence the onset position of upstream-CHF. Since the upstream-CHF phenomenon in this study was only observed at two different pressure levels and due to the limited number of data points obtained at a reduced pressure of $P_{red} = 0.95$ the influence of pressure cannot be investigated in detail. Therefore, the analysis focuses on mass flux and critical vapor quality under constant pressure conditions. To investigate the influence of the local critical vapor quality, Figure 12 presents the position of the onset of the boiling crisis z_{CHF} as a function of the local critical vapor quality x_{CHF} at various mass fluxes. It can be observed that at a mass flux of 300 kg/m²s, the initial position of the boiling crisis does not follow a clear trend. At mass fluxes of 600 kg/m²s and 1000 kg/m²s, no direct influence of the local critical vapor quality on the position of the boiling crisis at the onset of upstream-CHF could be identified either. Only at higher mass fluxes of 1500 kg/m²s and 2000 kg/m²s was a slight influence of the local critical vapor quality observed. In these cases, the critical position of the boiling crisis shifted upstream with decreasing local critical vapor quality. Overall, however, it can be concluded that the influence of the critical vapor quality on the position of the boiling crisis should be considered as relatively small. Furthermore, the figure shows that significantly fewer upstream-CHF points could be detected at lower mass fluxes.

Figure 13 shows the influence of mass flux on the critical position of the boiling crisis at constant inlet temperatures. It becomes evident that the critical position of the boiling crisis shifts further upstream as the mass flux increases. This effect is especially pronounced at lower inlet temperatures. This finding could explain why upstream-CHF was observed much further upstream in experiments reported in the literature. As shown in Table 1, the mass fluxes in those studies were in some cases significantly higher than those achieved in this study. However, higher mass fluxes could not be realized in this study due to the limited power of the transformer.

Furthermore, the results suggest a trend where higher pressures may facilitate the appearance of upstream-CHF even at lower mass fluxes, since literature primarily reports experiments conducted at comparatively low pressures, where upstream-CHF was detected at high mass fluxes. These results therefore support previous findings that upstream-CHF tends to occur under conditions of very high mass flux and low inlet quality.

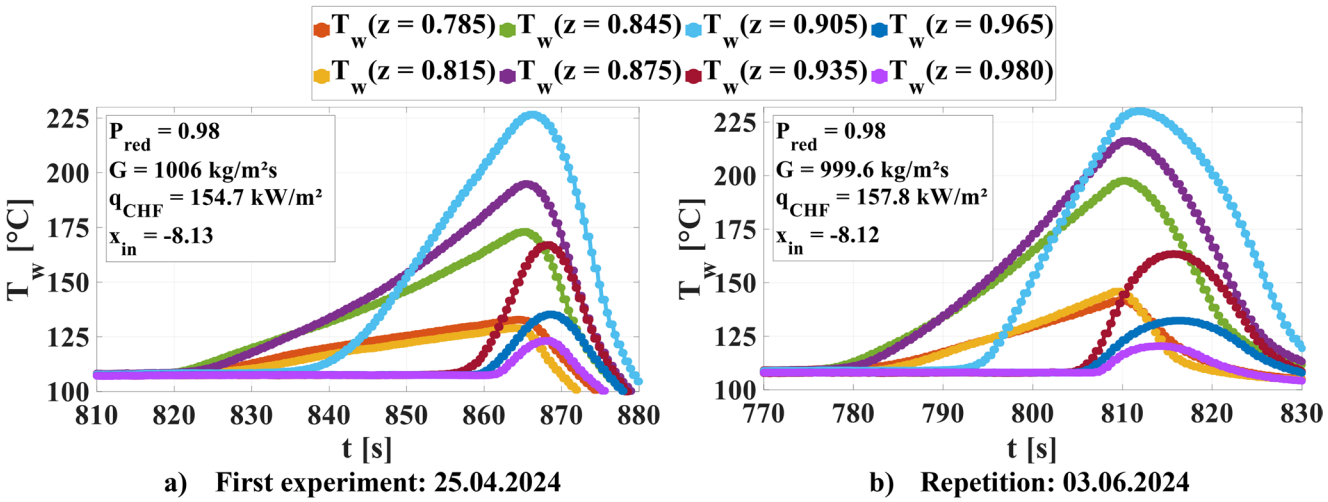

Fig. 11 Reproducibility of wall temperature development under upstream-CHF conditions

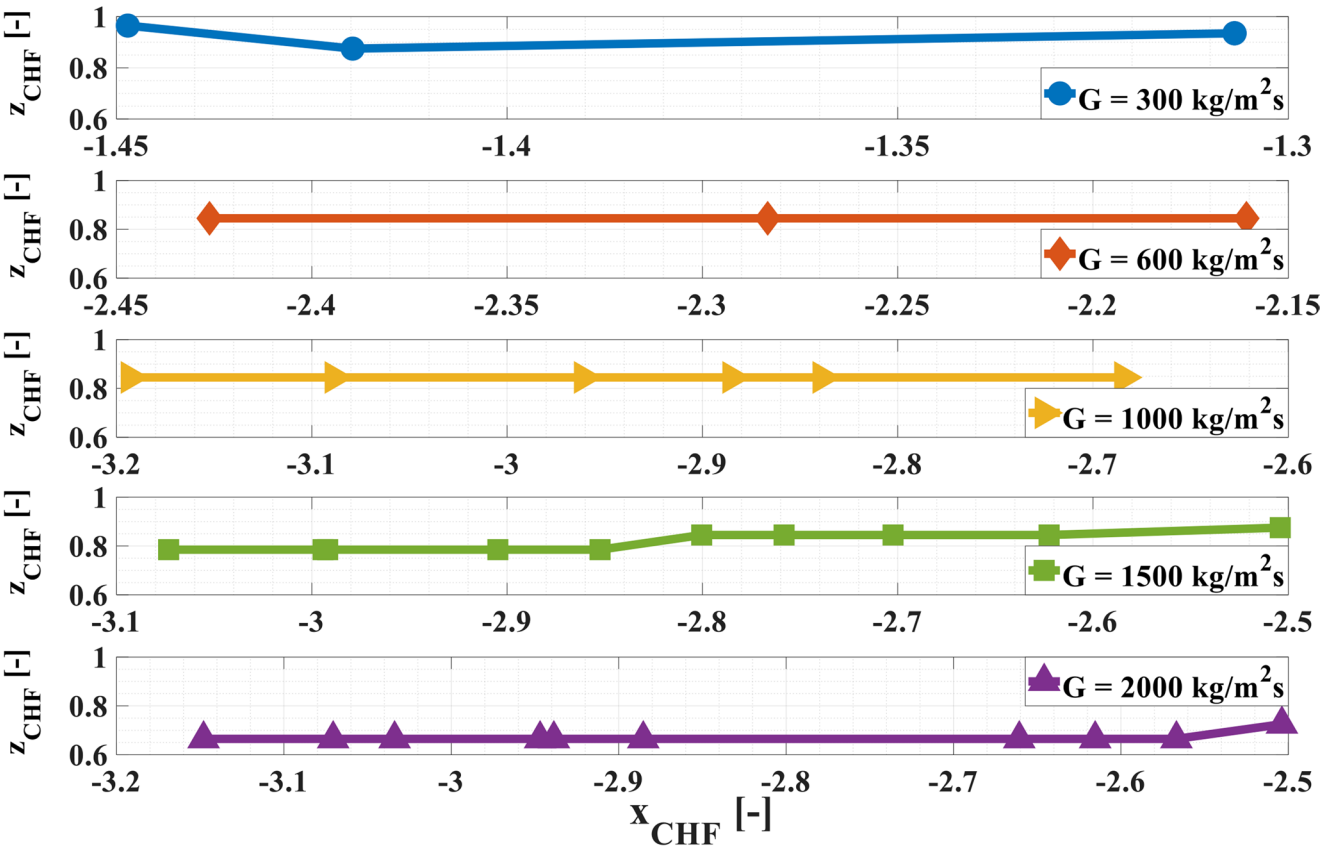

Fig. 12 Position of the boiling crisis z_{CHF} under upstream-CHF conditions as a function of critical vapor quality x_{CHF} at P_{red} = 0.98 and different mass fluxes

4.4 Possible reason and explanation for the development of upstream-CHF

Since the explanation of Groeneveld [12] is not further substantiated and a more detailed analysis of upstream-CHF data is lacking in the literature, a new possible explanation is proposed in this work. To explain the observed upstream-CHF behavior, the phenomenon of homogeneous nucleation is considered. This refers to the sudden vaporization of the liquid in the adjacent area to the heated wall as soon as a critical degree of superheat is exceeded. Homogeneous nucleation represents the lowest possible extension of a liquid state within the metastable region and occurs without any nucleation. In contrast, heterogeneous boiling, which is by far the more common form of boiling in practical applications, involves bubble formation triggered by existing nucleation sites. The following paragraph examines the behavior of the homogeneous nucleation temperature and its physical limitations. At constant system pressure, homogeneous nucleation represents the maximum achievable temperature of a liquid below the critical temperature at which no phase transition has yet occurred. Once this critical state is exceeded, phase change takes place abruptly, and the liquid suddenly vaporizes [32].

To determine the homogeneous nucleation temperature, the so-called spinodal line is widely used in literature. It marks the boundary between metastable and unstable states and considers the absolute stability limit of the liquid phase. Once this line is crossed, even the smallest density fluctuation leads to immediate phase separation without the need for nucleation. Lienhard et al. [33] analyzed experimental data and based on that, they developed Eq. (10) to describe the spinodal line. This equation allows the calculation of the homogeneous nucleation temperature T_{HN} for water as a function of system pressure $(T_{sat} \sim f(P))$ and the critical temperature T_c:

$$T_{HN} = T_{sat} + T_c \bullet \left(0.923 - \frac{T_{sat}}{T_c} + 0.077 \bullet \left(\frac{T_{sat}}{T_c}\right)^9\right) \quad (10)$$

If the given equation for the limit of liquid stability is plotted as a function of the reduced pressure, it becomes evident that the homogeneous nucleation temperature increases with rising pressure. However, when considering the difference between the homogeneous nucleation temperature (T_{HN})

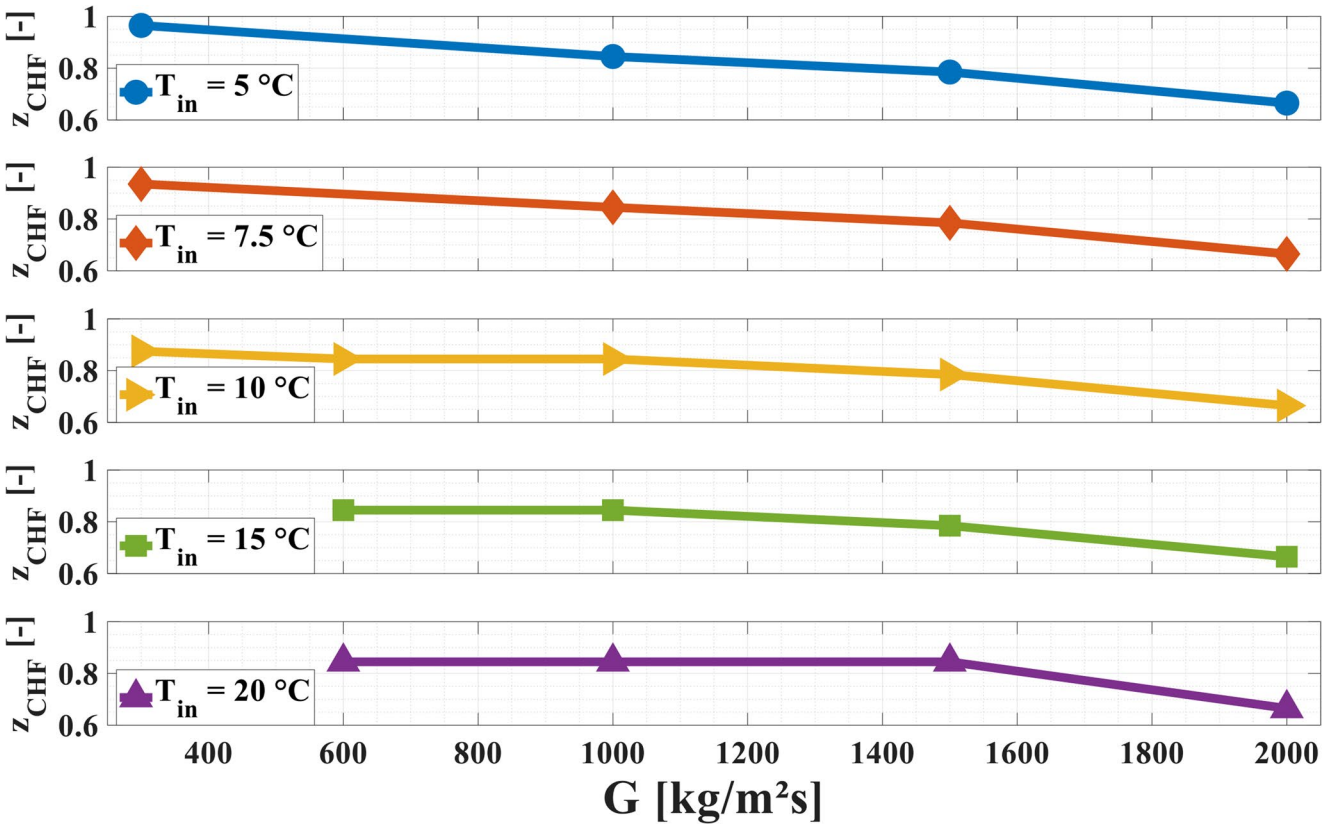

Fig. 13 Position of the boiling crisis z_{CHF} under upstream-CHF conditions as a function of mass flux G at P_{red} = 0.98 and different inlet temperatures

and the saturation temperature (T_{sat}), it becomes clear that this difference continuously decreases as pressure increases. The curve asymptotically approaches the saturation temperature and eventually reaches the critical temperature at the critical pressure, where the difference disappears entirely ($T_{sat}(P_c) = T_c = T_{HN}$).

To quantify this behavior for the present study, calculations based on Classical Nucleation Theory (CNT) combined with thermodynamic properties obtained from the fundamental equation of state by Tillner-Roth and Baehr [34] were performed. These calculations provide an estimate of the homogeneous nucleation temperature T_{HN} for the investigated pressure range.

The results indicate that at a high reduced pressure of $P_{red} = 0.95$, the estimated homogeneous nucleation temperature ($T_{HN} \approx 99.46\,°C$) is only about 0.9 °C above the saturation temperature ($T_{sat} \approx 98.53\,°C$). At $P_{red} = 0.98$, the difference becomes even smaller, with $T_{HN} \approx 100.57\,°C$ and $T_{sat} \approx 100.07\,°C$. These results illustrate that the metastable region of the liquid phase becomes extremely narrow as the system pressure approaches the critical pressure. Consequently, even small local temperature excursions may bring the liquid close to the limit of thermodynamic stability.

Figure 14a and 14b show exemplary temperature profiles at the inner surface of the heated wall immediately before the final power increase that leads to the occurrence of upstream-CHF. These illustrations represent the location of the upstream-CHF along the relative length, the saturation temperature and the estimated homogeneous nucleation temperature corresponding to the investigated pressure. In addition, the wall temperature profiles at different times after the onset of upstream-CHF are shown separately in the right-hand figures. It should be noted that the homogeneous nucleation temperature derived from CNT represents the thermodynamic stability limit of the liquid phase. In a flowing boiling system, however, the temperature of the liquid directly adjacent to the wall may differ from the calculated inner wall temperature due to convective transport, microlayer evaporation, and turbulent mixing effects. Consequently, the comparison between the calculated homogeneous nucleation temperature and the measured wall temperature should be interpreted qualitatively, indicating that the local thermodynamic conditions approach the stability limit of the liquid rather than representing an exact triggering condition for the onset of upstream-CHF.

If the heat flux increases further, the wall temperature at the previously identified local maximum continues to rise. Under such conditions, the thermodynamic state of the liquid adjacent

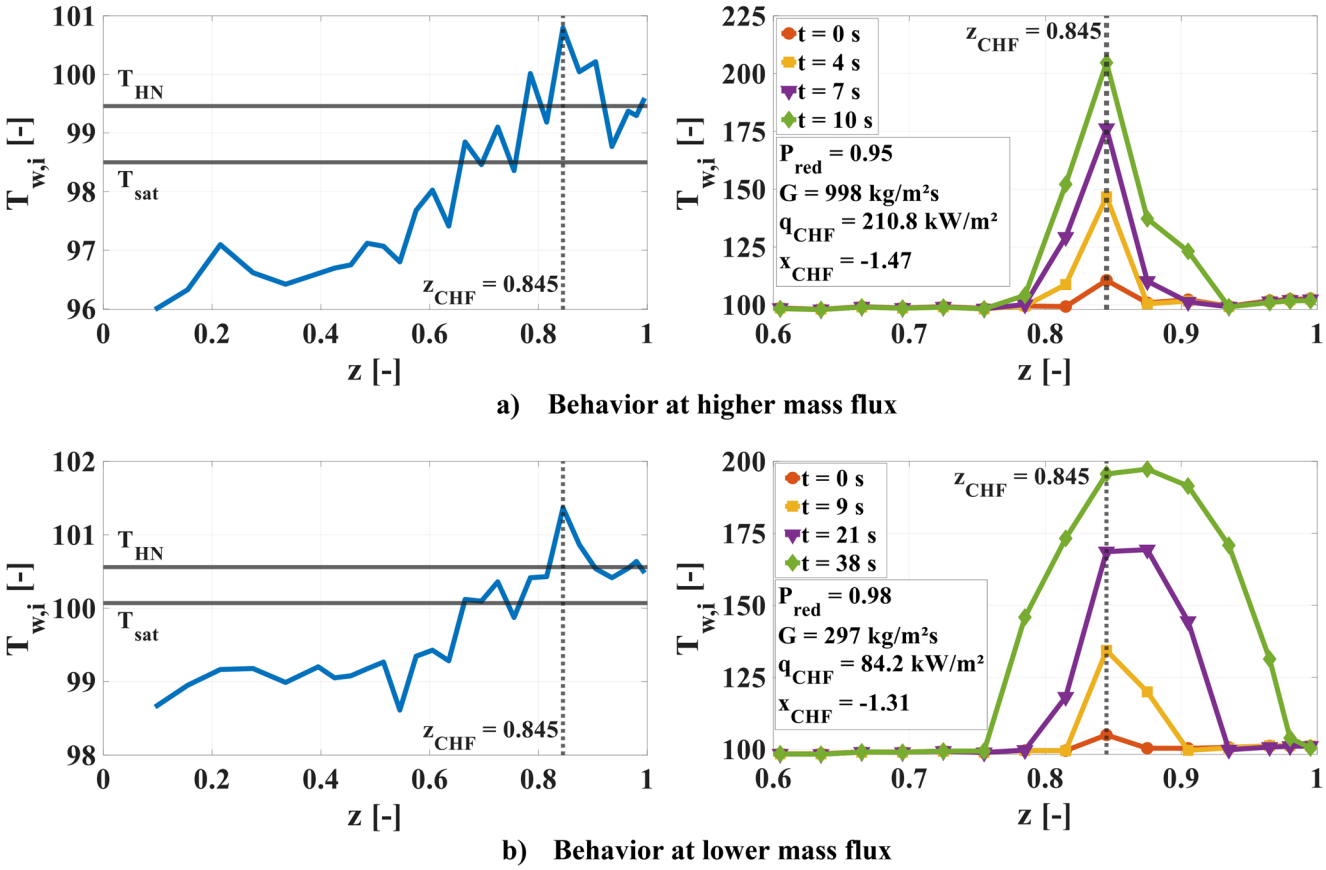

Fig. 14 Inner wall temperatures $T_{w,i}$ along the relative length z before the last heat flux increase (left) as well as the development during upstream-CHF (right) for different flow conditions

to the heated wall may approach the stability limit of the metastable liquid phase. According to classical nucleation theory, vapor bubbles may then form spontaneously. The rapid formation of vapor bubbles can lead to the development of a vapor layer that significantly reduces the local heat transfer from the wall to the fluid. As a consequence, the heated surface can no longer be cooled effectively, which results in the onset of boiling crisis and therefore in an increase in wall temperature. In the present experiments, this process appears at the axial location where the local wall temperature maximum is observed, thereby triggering the upstream-CHF phenomenon.

It is noteworthy that this local temperature maximum does not occur at the downstream end of the heated section but rather at the axial position where upstream-CHF later develops. The physical mechanism responsible for the formation of this upstream temperature peak could not be conclusively identified within the present study. However, the observed temperature profiles indicate that local thermodynamic conditions may develop upstream that favor the formation of metastable liquid states and the possible onset of homogeneous nucleation.

5 Summary

This paper presents an experimental investigation of the critical heat flux in a wide range of pressures and the observations of the upstream-CHF with R-134a in a vertically installed tube. A comprehensive database was obtained, with which the following results were found after detailed post-processing:

- It was presented that a change of the heated length from 3 m to 1 m consistently extends the CHF vs. critical vapor quality curve. The respective curves aligned almost seamlessly. Furthermore, it was shown that the CHF decreases almost linearly with the increase in the critical vapor quality.
- In addition, the influence of mass flux on CHF was investigated as a function of the local critical vapor quality. The results show that at strongly negative vapor qualities, where DNB-type mechanisms dominate, CHF generally increases with increasing mass flux. In contrast, at higher or slightly positive vapor qualities,

where dryout-type mechanisms become more relevant, the sensitivity of CHF to mass flux decreases. This trend is consistent with the inverse mass flux effect reported in the literature. It should be noted that under the high-pressure conditions investigated in this study, a strict distinction between DNB and dryout mechanisms becomes increasingly difficult.

- Also, the pressure influence on the CHF was investigated. It is obvious that pressure has a great influence on the CHF. In lower pressure region the influence of pressure was relatively small, but the CHF decreases more significantly at higher pressure. This can be explained by the dramatic change of the fluid properties near the critical pressure.
- Moreover, the so-called upstream-CHF was observed during the experiments, where the point of boiling crisis is shifted upstream the heated length. It was discovered that the boiling crisis spreads around the starting point, and the development of the phenomenon can be reproduced well. Besides that, it was shown that increasing mass flux as well as decreasing critical vapor quality shifts the starting point of the upstream-CHF further upstream.
- An explanation for the upstream-CHF phenomenon was proposed that considers the possible influence of homogeneous nucleation. The experiments revealed that the inner wall temperature profiles exhibit a local maximum before the occurrence of upstream-CHF. As the heat flux increases, the fluid adjacent to the heated wall reaches the metastable region of the liquid phase. Under such conditions, rapid vapor generation within the superheated liquid may become possible. The sudden formation of vapor bubbles can locally decrease the heat transfer and promote the formation of a vapor layer at the wall. As a result, the heated surface can no longer be cooled effectively, which leads to an onset of boiling crisis and therefore, to an increase in wall temperature. In the present experiments, this process appears to begin at the axial location where the local wall temperature maximum is observed, thereby triggering the upstream-CHF phenomenon.
- The identification of such local wall temperature maxima preceding upstream-CHF provides useful insight into the spatial development of boiling crisis under near-critical pressure conditions. These findings may support future experimental investigations and contribute to improving the understanding and modeling of upstream-CHF behavior in high-pressure boiling systems.

Appendix 1

Shah (LCC) correlation [29]:

$$
\begin{gathered}
q_{CHF} = Bo_{Shah} \bullet G \bullet h_{fg} \\
Bo_{Shah} = F_E \bullet F_x \bullet Bo_0 \\
F_E = \begin{cases} 1.54 - 0.032\left(\frac{L_{CHF}}{D_H}\right); F_E \geq 1 \\ 1 \qquad\qquad\qquad\quad ; F_E < 1 \end{cases} \\
Y = \left(\frac{G \bullet D_H \bullet C_{Pl}}{\lambda_l}\right)\left(\frac{G^2}{\rho_l \bullet g \bullet D_H}\right)^{0.4}\left(\frac{\mu_l}{\mu_v}\right)^{0.6} \\
Bo_0 = \max\left(Bo_{0,1},\ Bo_{0,2},\ Bo_{0,3}\right) \\
Bo_{0,1} = 15 \bullet Y^{-0.612} \\
Bo_{0,2} = 0.082 \bullet Y^{-0.3} \bullet \left(1 + 1.45 \bullet P_{red}^{4.03}\right) \\
Bo_{0,3} = 0.0024 \bullet Y^{-0.105} \bullet \left(1 + 1.15 \bullet P_{red}^{3.39}\right)
\end{gathered}
\tag{A1}
$$

for $x_{CHF} > 0$:

$$
\begin{gathered}
c_{Shah} = \begin{cases} 0 \ ; \ P_{red} \leq 0.6 \\ 1 \ ; \ P_{red} > 0.6 \end{cases} \\
F_3 = \left(\frac{1.25 \bullet 10^5}{Y}\right)^{0.833 \bullet x_{CHF}} \\
F_x = F_3 \bullet \left[1 + \frac{\left(F_3^{-0.29} - 1\right) \bullet \left(P_{red} - 0.6\right)}{0.35}\right]^{c_{Shah}}
\end{gathered}
$$

for $x_{CHF} \leq 0$:

$$
\begin{gathered}
b_{Shah} = \begin{cases} 0 \ ; \ P_{red} \leq 0.6 \\ 1 \ ; \ P_{red} > 0.6 \end{cases} \\
F_1 = \begin{cases} 1 + 0.0052 \bullet \left[\left(-x_{CHF}\right)^{0.88}\right] \bullet Y^{0.41} & ; \ Y \leq 1.4 \bullet 10^7 \\ 1 + 0.0052\left[\left(-x_{CHF}\right)^{0.88}\right] \bullet \left(1.4 \bullet 10^7\right)^{0.41} & ; \ Y > 1.4 \bullet 10^7 \end{cases} \\
F_2 = \begin{cases} F_1^{-0.42} \ ; \ F_1 \leq 4 \\ 0.55 \ ; \ F_1 > 4 \end{cases} \\
F_x = F_1\left[1 - \frac{(1 - F_2) \bullet \left(P_{red} - 0.6\right)}{0.35}\right]^{b_{Shah}}
\end{gathered}
$$

Song correlation [30]:

$$
\begin{gathered}
q_{CHF} = Bo_{Song} \bullet G \bullet h_{fg} \\
Bo_{Song} = f\left(We_v\right) \bullet f\left(x_{CHF}\right) \\
We_v = \frac{G^2 \bullet D_H}{\rho_v \bullet \sigma} \\
f\left(We_v\right) = \max\left(A_1,\ A_2\right) \\
f\left(x_{CHF}\right) = \left(B_1 + B_2 + B_3\right) - \max\left(B_1, B_2,\ B_3\right) - \min\left(B_1,\ B_2,\ B_3\right) \\
A_1 = 7.796 \bullet 10^{-2} \bullet We_v^{-0.4388} \\
A_2 = 1.530 \bullet 10^{-3} \bullet We_v^{-0.0803} \\
B_1 = 2.156 \bullet \left(1 - x_{CHF}\right)^{0.688} \\
B_2 = 1.841 \bullet \left(1 - x_{CHF}\right)^{2.137} \\
B_3 = 0.672 \bullet \left(1 - x_{CHF}\right)^{0.219}
\end{gathered}
\tag{A2}
$$

Equations for the statistical evaluation:

$$
E_{j,cor} = \frac{q_{CHF_{j,cor}} - q_{CHF_{j,meas}}}{q_{CHF_{j,meas}}} \tag{A3}
$$

$$
ME = \frac{1}{N}\sum_{j=1}^{N} E_{j,cor} \tag{A4}
$$

$$MAE = \frac{1}{N} \sum_{j=1}^{N} |E_{j,cor}| \tag{A5}$$

$$RMS = \sqrt{\frac{1}{N} \sum_{j=1}^{N} E_{j,cor}^2} \tag{A6}$$

Acknowledgements The authors would like to thank the German Federal Ministry of Research, Technology and Space (BMFTR, CPC-HD Project, Grant No. 02NUK062A) for providing the financial support for this study.

Author contributions The first draft of the manuscript was written by Nikolai Rensch and all authors commented on previous versions of the manuscript. All authors read and approved the final manuscript.

Funding Open Access funding enabled and organized by Projekt DEAL. The authors would like to thank the German Federal Ministry of Research, Technology and Space (BMFTR, CPC-HD Project, Grant No. 02NUK062A) for providing the financial support for this study.

Data availability The used data was generated within the CPC-HD Project with the Grant No. 02NUK062A. Aside from the data published in this manuscript, the data connot be published further, as it belongs to the project and is not avialable to the public.

Declarations

Competing interests The authors declare no competing interests.

References

1. Habib MA, Nemitallah MA, El-Nakla M (2014) Current status of CHF predictions using CFD modeling technique and review of other techniques especially for non-uniform axial and circumferential heating profiles. Ann Nucl Energy 70:188–207. https://doi.org/10.1016/j.anucene.2014.03.016
2. Tong LS, Tang YS Boiling Heat Transfer and Two-Phase Flow, Series in Chemical and Mechanical Engineering, Second Edition., Washington DC (1997) USA: Taylor & Francis. https://doi.org/10.1201/9781315138510
3. Vijayarangan BR, Jayanti S, Balakrishnan AR (2006) Studies on critical heat flux in flow boiling at near critical pressures. Int J Heat Mass Transf 49(1–2):259–268. https://doi.org/10.1016/j.ijheatmasstransfer.2005.06.029
4. Goldmann K, Firstenberg H, Lombardi C (1960) Burnout in Turbulent Flow - A Droplet Diffusion Model, 60-HT-34, Heat Transfer Division of the American Society of Mechanical Engineers at the ASME-AIChE Heat Transfer Conference, Buffalo, New York, August 16–17, pp. 1–8
5. Groeneveld DC, Delorme GGJ (1976) Prediction of thermal non-equilibrium in the post-dryout regime. Nucl Eng Des 36(1):17–26. https://doi.org/10.1016/0029-5493(76)90138-2
6. Dahariya S, Betz AR (2019) High pressure pool boiling: mechanisms for heat transfer enhancement and comparison to existing models. Int J Heat Mass Transf 141:696–706. https://doi.org/10.1016/j.ijheatmasstransfer.2019.07.016
7. Hong SD, Chun SY, Yoon YJ, Baek WP (2003) Heat Transfer Characteristics of R-134a Fluid during the Pressure Transient from Supercritical Pressure to Subcritical Pressure. In *Proceedings of the 10th International Topical Meeting on Nuclear Reactor Thermal Hydraulics (NURETH-10)*. Seoul Korea: 5.-1. October, 2003
8. Zhu X, Bi Q, Yang D, Chen T (2009) An investigation on heat transfer characteristics of different pressure steam-water in vertical upward tube. Nucl Eng Des 239(2):381–388. https://doi.org/10.1016/j.nucengdes.2008.10.026
9. Nishikawa K, Yoshida S, Yamada A, Ohno M (1982) Experimental Investigation of Critical Heat Flux in Forced Convection Boiling of Freon in a tube at High Subcritical Pressure, In *Proceedings of the 7th International Heat Transfer Conference.* Munic, Germany: 6.-10. September, 1982. Pp. 321–326
10. Kitto JB (2021) Upstream critical heat flux and its design implications. Heat Transf Eng 43(6):475–484. https://doi.org/10.1080/01457632.2021.1887623
11. Waters ED, Anderson JK, Batch JM (1962) Experimental Observations of Upstream Boiling Burnout, HW-73902. General Electric Co, Hanford Atomic Products Operation, Richland, Washington, USA
12. Groeneveld DC (1975) The occurrence of upstream dryout in uniformly heated channels, Atomic Energy of Canada Ltd., Chalk River, Ontario. Chalk River Nuclear Labs., In Proceeding: 5th international heat transfer conference., Tokyo, Japan, September 3
13. Groeneveld DC (2011) Anomalies and other concerns related to the critical heat flux. Nucl Eng Des 241(11):4604–4611. https://doi.org/10.1016/j.nucengdes.2010.09.016
14. Bertoletti S, Gaspari GP, Lombardi C, Soldaini G, Zavattarelli R (1964) Heat Transfer Crisis in Steam-Water Mixtures -- Experimental Data in Round Tubes and Vertical Upflow Obtained During the Can-2 Program, EURAEC-1084. Centro Informazioni Studi Esperienze, Milan, Italy
15. Hassid A, Mazoni GC, Ravetta R, Rubiera L (1966) Heat Transfer Crisis in Steam-Water Mixtures: An Experimental Study on the Increase if Critical Power with Local Swirl Promoters in Round Tubes, CISE-R-169. Centro Informazioni Studi Esperienze, Milan, Italy
16. Merilo M (1977) Critical heat flux experiments in a vertical and horizontal tube with both freon-12 and water as coolant. Nucl Eng Des 44(1):1–16. https://doi.org/10.1016/0029-5493(77)90119-4
17. Merilo M, Ahmad SY (1979) Experimental study of CHF in vertical and horizontal tubes cooled by freon-12. Int J Multiph Flow 5(6):463–478. https://doi.org/10.1016/0301-9322(79)90032-6
18. Katto Y, Ashida S (1982) CHF in High-Pressure Regime for Forced Convection Boiling in Uniformly Heated Vertical Tubes of Low Length-to-Diameter Ratio, Department of Mechanical Engineering, University of Tokyo, In Proceeding: 7th international heat transfer conference., Germany, Munich, September 6–10
19. Yokoya S, Watanabe M, Shoji M (1996) Upstream critical heat flux of forced convection boiling inside a uniformly heated vertical tube. Trans Japan Soc Mech Eng Ser B 62(597):1898–1905
20. VDM Metals International (2020) VDM Alloy 625: Nicrofer 6020 hMo, Data Sheet No. 4118, Revision 04. Werdohl, Germany

21. Lemmon EW, Bell IH, Huber ML, McLinden MO (2018) Nist standard reference database 23: Reference fluid thermodynamic and transport properties - refprop, version 10. Tech. Rep.), National Institute of Standards and Technology
22. Groeneveld DC, Snoek CW (1986) A comprehensive examination of heat transfer correlations suitable for reactor safety analysis. Multiph Sci Technol 2(1–4):181–274
23. Pioro IL, Groeneveld DC, Cheng SC, Doerffer S, Vasic AZ, Antoshko YV (2001) Comparison of CHF measurements in R-134a cooled tubes and the water CHF look-up table. Int J Heat Mass Transf 44(1):73–88. https://doi.org/10.1016/S0017-9310(00)00093-4
24. Cheng X, Müller U (2003) Review on Critical Heat Flux in Water Cooled Reactors. Institut für Kern- und Energietechnik, Wissenschaftlicher Bericht, FZKA 6825, Forschungszentrum Karlsruhe GmbH, Germany
25. Mudawar IA, Bowers MB (1999) Ultra-high critical heat flux (CHF) for subcooled water flow boiling—I: CHF data and parametric effects for small diameter tubes. Int J Heat Mass Transf 42(8):1405–1428. https://doi.org/10.1016/S0017-9310(98)00241-5
26. Celata GP, Mariani A, ENEA (1999) Critical heat flux, post dry-out and their augmentation. Dipartimento Energia, RT/ERG/98/10, Centro Ricerche Casaccia, S. Maria di Galeria, Roma, Italy
27. Chun SY, Hong SD, Kikura H, Aritomi M (2007) Critical heat flux in a heater rod bundle cooled by R-134a fluid near the critical pressure. Journal of Nuclear Science and Technology 44(9):1189–1198. https://doi.org/10.1080/18811248.2007.9711362
28. Pioro IL, Cheng SC, Vasic AZ, Salah I (1999) Experimental evaluation of the limiting critical quality values in circular and non-circular flow geometries. Nucl Eng Des 190(3):317–339. https://doi.org/10.1016/S0029-5493(99)00077-1
29. Shah MM (1987) Improved general correlation for critical heat flux during upflow in uniformly heated vertical tubes. Int J Heat Fluid Flow 8(4):326–335. https://doi.org/10.1016/0142-727X(87)90069-5
30. Song M, Liu X, Cheng X (2021) Prediction of critical heat flux (CHF) for the high-pressure region in uniformly heated vertical round tubes. Annals of Nuclear Energy 158:108303. https://doi.org/10.1016/j.anucene.2021.108303
31. Groeneveld DC (1972) The Thermal Behaviour of a Heated Surface At and Beyond Dryout, AECL-4309. Chalk River Nuclear Laboratories, Atomic Energy of Canada Limited, Chalk River, Ontario
32. Avedisian CT (1985) The homogeneous nucleation limits of liquids. J Phys Chem Ref Data 14(3):695–729. https://doi.org/10.1063/1.555734
33. Lienhard JH, Shamsundar N, Biney PP (1986) Spinodal lines and equations of state: a review. Nucl Eng Des 95:297–314. https://doi.org/10.1016/0029-5493(86)90056-7
34. Tillner-Roth R, Baehr HD (1994) An International Standard Formulation for the thermodynamic properties of 1,1,1,2-Tetrafluoroethane (HFC-134a) for temperatures from 170 K to 455 K and pressures up to 70 MPa. J Phys Chem Ref Data 23(5):657–729. https://doi.org/10.1063/1.555958